Multi-objective Thermal Optimization of Dual-input Aeronautic Static Inverter Based on MOEA/D

YAN Jie[1], *GE Hongjuan*[1*], *WANG Yongshuai*[2], *LI Huang*[1]

1. College of Civil Aviation, Nanjing University of Aeronautics and Astronautics, Nanjing 211106, P. R. China;
2. College of Automation, Nanjing University of Aeronautics and Astronautics, Nanjing 211106, P. R. China

(Received 8 April 2022; revised 11 August 2022; accepted 30 August 2022)

Abstract: To solve the multi-variable and multi-objective optimization problem in the thermal design process of the dual-input aeronautic static inverter, an optimization method based on the combination of the multi-objective evolutionary algorithm based on decomposition (MOEA/D) and the fuzzy set theory is proposed. The heat transfer path of the power device is analyzed and an equivalent heat circuit is conducted. We take junction temperature of the power device, mass, and cost of the heat sink as optimization goals, and take the heat sink structure parameters as design variables to conduct thermal optimization based on MOEA/D. This paper carries out a comparative study, and the results show that the proposed improved algorithm can meet the different requirements for multi-objective weights, and have good rapidity and robustness.

Key words: aeronautic static inverter; thermal optimization; heat sink; MOEA/D; fuzzy set theory

CLC number: TM46 **Document code**: A **Article ID**: 1005-1120(2022)S-0065-08

0 Introduction

Aeronautic static inverter (ASI) converts the electrical energy of generators or batteries into constant-frequency alternating current to provide high-quality electrical energy for electrical equipment of flight control and instrumentation. It is an important part of the aviation power system[1]. The dual-input structure can provide multi-level output characteristics and improve the overall conversion efficiency of the system, and is widely used in ASI circuit design[2]. But the increase of dual-input ASI power devices makes thermal failures one of the main reasons for equipment damages. The traditional thermal design which generally only needs to meet the basic heat dissipation performance, is often completed by engineers' combining experiences. However, with the continuous maturation of aircraft structure and functions, the small size and light weight of airborne equipment have become the main design goals, and traditional design methods obviously cannot achieve the optimal strategy.

Heat sink optimization is a multi-variable and multi-objective problem under constrained conditions[3-4]. The performance of the heat sink is related to the length, width, fin height, fin thickness, fin spacing, fin shape, and substrate thickness. Relationships with these parameters are often non-linear. Most scholars use thermal simulation software such as ANSYS to build a model to simulate the heat conduction process, which can intuitively obtain the temperature distribution of the components in the cooling system[5-6]. The result of this method is the most reliable, but adjusting the parameters within the constraints requires re-solving the model, which makes it difficult to estimate the overall calculation amount and time, and complex models will also increase the difficulty of modeling and the solution time. Therefore, some intelligent algorithms are needed to effectively search for the optimal value.

*Corresponding author, E-mail address: allenge@nuaa.edu.cn.

How to cite this article: YAN Jie, GE Hongjuan, WANG Yongshuai, et al. Multi-objective thermal optimization of dual-input aeronautic static inverter based on MOEA/D[J]. Transactions of Nanjing University of Aeronautics and Astronautics, 2022, 39(S): 65-72.

http://dx.doi.org/10.16356/j.1005-1120.2022.S.009

Refs.[4, 7] established optimization models that take the thermal resistance, heat transfer coefficients, or other heat sink performances as the objective function, and use a genetic algorithm for the single-objective optimization. This method is simple and reliable, but ignores the connection between multiple objectives and they cannot co-evolve, resulting in limited engineering applications.

This paper aims at the most widely used finned heat sink, and sets the junction temperature of the power device, the weight, and the cost of the heat sink as objective functions. We study the Pareto solution set based on MOEA/D and the objective function normalization, use the fuzzy set theory combined with required target weights to evaluate the satisfaction of the Pareto set, and obtain the compromise solution corresponding to the highest satisfaction. Then ANSYS Icepak software simulation is conducted to verify the accuracy of the proposed algorithm. The proposed method can provide a reference idea for the thermal design of ASI or other equipment.

1 Thermal Loss Analysis of Dual-input ASI Power Devices

1.1 Power device heat transfer path

To overcome the shortcomings of the traditional ASI that requires dead time and low conversion efficiency, LI et al.[2] proposed a three-phase dual-input dual-buck inverter structure. This circuit uses reverse diodes to completely eliminate the bridge arm through risks, and part of the power is directly provided by the low-voltage DC input source, reducing the number of power conversion stages. In this topology, the power devices are composed of MOSFET switch tubes and diodes, as shown in Fig.1.

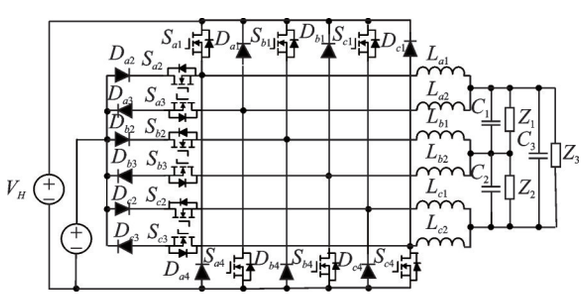

Fig.1 Three-phase dual-input dual-buck inverter topology

As shown in Fig.2, when the power devices are working normally, their internal semiconductor chip is the main source of heat. This temperature is called junction temperature. The heat is transferred to the substrate of the heat sink by solid heat conduction through intermediate media such as solder and thermal silica. And then through the fins of the heat sink, it is transferred into the air in a solid-flow heat conduction mode.

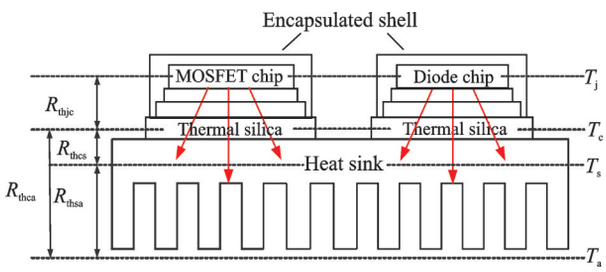

Fig.2 Heat transfer path of power devices

In Fig.2, R_{thjc} is the junction-case thermal resistance; R_{thca} the device case-air thermal resistance; R_{thcs} the case-heat sink thermal resistance; and R_{thsa} the heat sink-air thermal resistance. T_j, T_c, T_s and T_a are the temperature of the junction, case, heat sink, and ambient, respectively.

1.2 Power device temperature function solution

The dissipated power is equivalent to the current source. The temperature at each point is equivalent to the voltage. The temperature difference is equivalent to the voltage drop, and the thermal resistance is equivalent to the resistance[8]. According to the heat transfer path shown in Fig.2, the thermal resistance equivalent circuit of the power devices and the heat sink are obtained, as shown in Fig.3.

The temperature expression of each point in the cooling system can be obtained as

$$\begin{cases} T_s = P_{tot} \times R_{thsa} + T_a \\ T_c = P_{tot} \times R_{thcs} + T_s \\ T_{j\_S} = P_S \times R_{thjc\_S} + T_c \\ T_{j\_D} = P_D \times R_{thjc\_D} + T_c \end{cases} \tag{1}$$

where P_S and P_D are the power loss of the switch tube and the diode, respectively; $P_{tot}=P_S+P_D$ is the total loss of the power devices; R_{thjc} is related to the performance of the power device; R_{thcs} depends

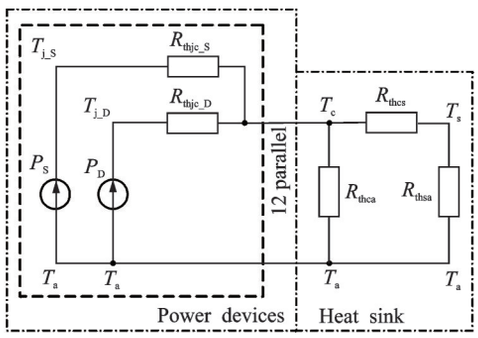

Fig.3 Thermal resistance equivalent circuit of power devices and heat sink

on the contact surface of the power device and the heat sink, which can be obtained from the manual; R_{thca} is much larger than R_{thcs} and R_{thsa}, and can be ignored when connected in parallel.

Therefore, the equivalent thermal resistance of the cooling system can be expressed as

$$\begin{cases} R_{thja\_S} = R_{thjc\_S} + R_{thcs} + R_{thsa} \\ R_{thja\_D} = R_{thjc\_D} + R_{thcs} + R_{thsa} \end{cases} \tag{2}$$

Then, the expressions for the junction temperature of the switch tube and the diode can be obtained as

$$\begin{cases} T_{j\_S} = P_S R_{thjc\_S} + P_{tot} R_{thcs} + P_{tot} R_{thsa} + T_a \\ T_{j\_D} = P_D R_{thjc\_D} + P_{tot} R_{thcs} + P_{tot} R_{thsa} + T_a \end{cases} \tag{3}$$

2 Determination of Objective Function of Heat Sink

A typical heat sink is composed of several thinner fins and a thicker base. The fins are arranged with a certain gap and connected to the substrate to increase the overall heat dissipation area. The base is attached to the surface of the heat source. In Fig.4, H, W, and t_b are the length, the width, and the height of the base, respectively, and W_a, W_b, and L are the thickness, the spacing, and the height of the fins.

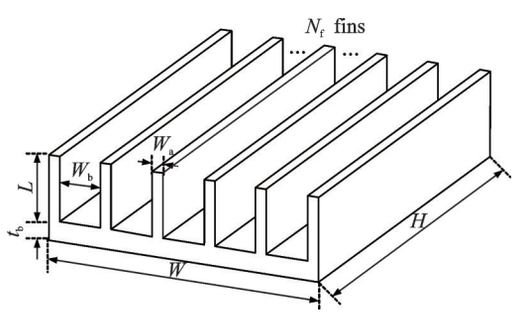

Fig.4 Schematic diagram of finned heat sink structure

The heat sink total thermal resistance is the sum of the convection-radiation thermal resistance, base conduction thermal resistance, spreading thermal resistance, and caloric thermal resistance.

$$R_{thsa} = R_{cr} + R_b + R_s + R_c \tag{4}$$

The convection-radiation thermal resistance is

$$R_{cr} = \frac{1}{\left[1 - \frac{N_f A_f}{A_t}(1 - \eta_f)\right] h A_t} \tag{5}$$

where N_f is the number of fins; A_f the fin area; A_t the total heat sink area; h the combined radiation and convection heat transfer coefficient; $\eta_f = \tan aL_c/(aL_c)$ the fin efficiency; $L_c = L + A_c/P$ the fin corrected length; $a^2 = hP/(kA_c)$; A_c the cross-section area; P the cross-section perimeter, and k the thermal conductivity of the heat sink.

The base conduction thermal resistancise

$$R_b = \frac{t_b}{kWH} \tag{6}$$

The spreading thermal resistance[9] exists in the process of heat transfer from surfaces with unequal areas.

$$R_s = \frac{(1 - \varepsilon)\phi}{\pi k r_1} \tag{7}$$

$$\phi = \frac{\tanh(\lambda\tau) + \frac{\lambda}{Bi}}{1 + \frac{\lambda}{Bi}\tanh(\lambda\tau)} \tag{8}$$

where $\lambda = \pi + 1/\varepsilon\sqrt{\pi}$, $Bi = h_{eff} r_2/k$, $h_{eff} = 1/R_{cr}A_s$, $\tau = t_b/r_2$, $\varepsilon = r_1/r_2$, $r_1 = \sqrt{A_{th}/\pi}$, $r_2 = \sqrt{A_s/\pi}$, A_{th} the area of the heat source, and A_s the area of the contact surface between the base and the heat source.

Assuming that the fluid mass flow rate through the heat sink is m_a, and the fluid-specific heat at constant pressure is C_p, the heat sink caloric thermal resistance is given by

$$R_c = \frac{1}{2m_a C_p} \tag{9}$$

The cost of the heat sink depends on the size and spacing of the fins, the heat sink material, weight, the output, and so on. The material of the heat sink is fixed, and the fin thickness and the fin height-to-width ratio (L/W_b) are selected as cost

factors, which are inverse and direct

$$S = k_1 \frac{1}{W_a} + k_2 \frac{L}{W_b} \tag{10}$$

where k_1 and k_2 are the weights of the influence of the fin thickness and the fin height-to-width ratio on the cost, respectively.

It should be noted that S here is only a dimensionless value that characterizes the cost. In order to balance the difference between W_a and L/W_b, it is normalized.

$$S = k_1 \cdot \frac{1/W_a - (1/W_a)_{\min}}{(1/W_a)_{\max} - (1/W_a)_{\min}} + k_2 \cdot \frac{L/W_b - (L/W_b)_{\min}}{(L/W_b)_{\max} - (L/W_b)_{\min}} \tag{11}$$

Assuming that ρ is the density of heat sink, weight can be expressed as

$$m = \rho \cdot (NLW_a + Wt_b) \cdot H \tag{12}$$

3 Thermal Optimization Design Based on MOEA/D

3.1 MOEA/D Algorithm

The MOEA/D algorithm[10-11] transforms the multi-objective optimization problem into a series of single-objective optimization sub-problems. A certain number of adjacent problem information is used to optimize these sub-problems at the same time. Due to the decomposition operation, this method has a great advantage in maintaining the distribution of the solution.

This paper chooses the Tchebycheff aggregation method, in which each sub-problem can be expressed as

$$\min g^{te}(x|\lambda, z^*) = \max_{1 \leqslant j \leqslant m} \left\{ \lambda_j | f_i(x) - z_j^* \right\} \tag{13}$$

where $z^* = \min \left\{ f_i(x) | x \in \Omega \right\}$, $i \in \{1, 2, \cdots, m\}$ is the reference point of the ith dimension target, and λ is the weight; m the number of objective functions.

3.2 Improvement of MOEA/D

The Tchebycheff method calculates the product of the weight and the difference between the target value and the ideal point, and then evolves in the direction of reducing the maximum difference to achieve continuous approximation to the ideal point on a single sub-problem. However, multiple objective functions often have different measurement units. For example, the cost and the junction temperature in this paper are different in values by two orders of magnitude, which will cause the junction temperature continues to decrease. And the optimal frontier obtained at this time is not uniformly distributed, which cannot provide a representative optimal solution. In order to solve the problems, this paper normalizes each objective function

$$f_i' = \frac{f_i - f_{\min i}}{f_{\max i} - f_{\min i}} \tag{14}$$

where f_i, f_i', $f_{\max i}$, $f_{\min i}$ are the true value, the normalized value, the maximum value, and the minimum value of the ith dimension objective function, respectively.

In fact, users do not want to spend time processing Pareto optimal solutions. In order to select some compromise solutions among these N solutions, the fuzzy set theory proposed in Ref.[12] is used to quantitatively evaluate each optimal solution. First, the satisfaction of each target in the kth Pareto solution in that dimension is evaluated

$$\mu_i^k = \begin{cases} 1 & f_i^k \leqslant f_{\min i} \\ \dfrac{f_{\max i} - f_i^k}{f_{\max i} - f_{\min i}} & f_{\min i} < f_i^k < f_{\max i} \\ 0 & f_i^k \geqslant f_{\max i} \end{cases} \tag{15}$$

where f_i^k is the function value of the kth Pareto solution on the ith dimensional objective function.

Then, where the final satisfaction of the kth Pareto solution is evaluated

$$\mu^k = \sum_{i=1}^{m} c_i \mu_i^k \Big/ \left(\sum_{q=1}^{N} \sum_{i=1}^{m} c_i \mu_i^q \right) \tag{16}$$

where N is the number of Pareto optimal solutions, and c_i the weight of the ith dimension objective set artificially. Finally, the solution with the greatest satisfaction is selected as the compromise solution.

4 Thermal Optimization Application Based on MOEA/D

4.1 Optimal parameter and constraint setting

In the circuit shown in Fig.1, P_{tot}=48.275 1 W. The junction temperature of the switch tube S_{a4} with the largest power loss P_{Sa4}=4.601 6 W is selected

as one of the objective functions. The maximum allowable junction temperature is T_{jmax}=175 ℃. The maximum allowable temperature is 125 ℃ after derating.

We set R_{thjc}=0.44 ℃/W by consulting the product manual, R_{thcs}=0.013 ℃/W, and choose the aluminum heat sink with thermal conductivity k=2.08 W/(cm·℃). We set the heat sink cost coefficient k_1=0.4, k_2=0.6, ambient temperature T_a=25 ℃, air natural convection heat transfer coefficient h=10, the chip package side length of 10 mm. The size constraints of the heat sink are shown in Table 1.

Table 1 Heat sink size constraints

Size parameter	Restriction/mm	Size parameter	Restriction/mm
W_a	1—5	W_b	2—8
W	70—140	H	200—280
t_b	5—10	L	30—80

According to Eqs.(3,11,12), the optimization model is obtained.

$$\min: \ T_j, m, S = f(W_a, W_b, W, H, t_b, L) \tag{17}$$

The constraints are

$$\begin{cases} T_j \leqslant 125\ ℃ \\ X_{i,\min} \leqslant X_i \leqslant X_{i,\max} \end{cases} \tag{18}$$

where X_i is size parameters of the heat sink.

4.2 Analysis of optimization results

This paper selects four sets of compromise solutions for the user. The optimization results are shown in Figs.5, 6 and Table 2. It can be seen from Fig.5(a) that the decrease in the mass of the heat sink leads to an increase in the junction temperature.

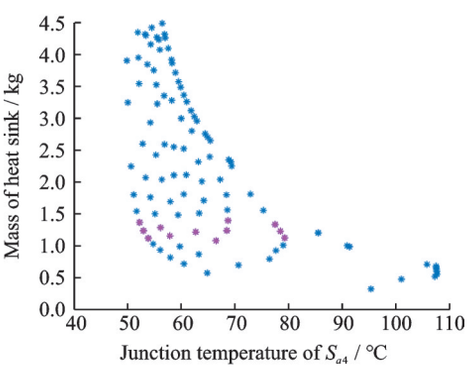

(a) Relationship between junction temperature of S_{a4} and weight of heat sink

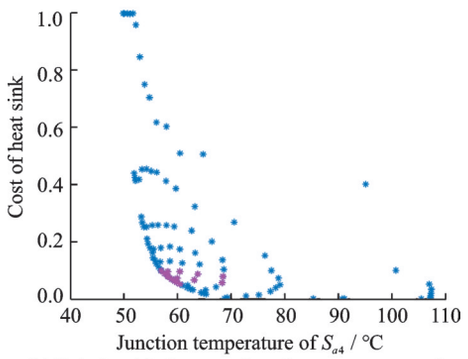

(b) Relationship between junction temperature of S_{a4} and cost of heat sink

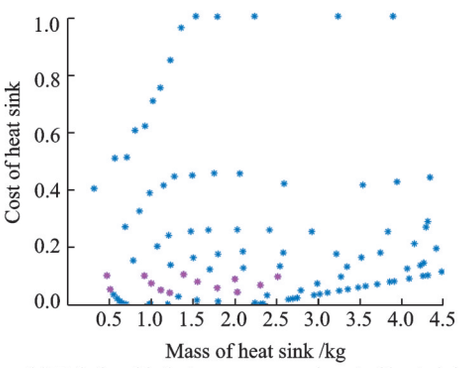

(c) Relationship between mass and cost of heat sink

Fig.5 MOEA/D optimization frontier 2D map

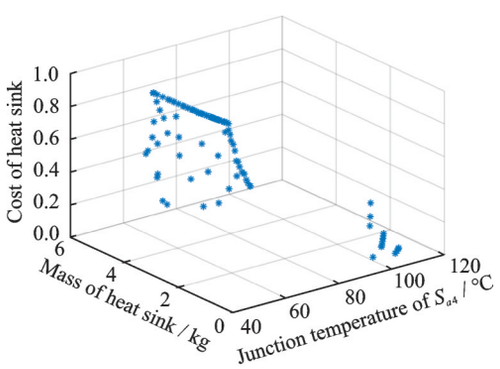

(a) Unnormalized optimization frontier

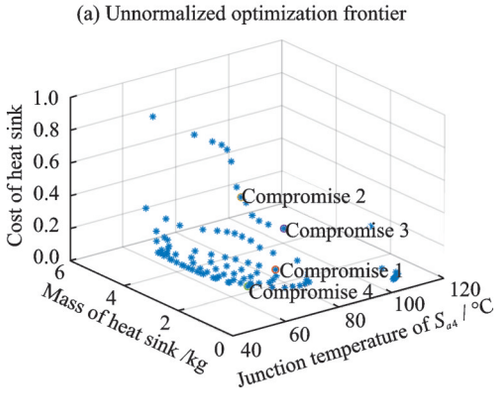

(b) Normalized optimization frontier

Fig.6 MOEA/D optimization frontier 3D map

Within the mass of 1—1.5 kg, there is a phenomenon that the junction temperature continues to decrease but the increase in the mass is not obvious.

Table 2 Pareto compromise solution of MOEA/D

Optimization result		Compromise 1: (c_1, c_2, c_3)= (1/3, 1/3, 1/3)	Compromise 2: (c_1, c_2, c_3)= (0.7, 0.2, 0.1)	Compromise 3: (c_1, c_2, c_3)= (0.2, 0.7, 0.1)	Compromise 4: (c_1, c_2, c_3)= (0.2, 0.1, 0.7)
Objective function	T/℃	66.061 6	54.711 9	64.816 0	69.324 3
	m/kg	1.024 9	1.033 8	0.572 3	2.307 5
	S	0.220 3	0.709 4	0.500 1	0
Design variables/mm	W_a	2.3	1	1	5
	W_b	8	3.6	8	8
	W	70	70	70	140
	H	200	200	200	280
	t_b	8.6	9	6.2	10
	L	80	80	78.4	30

This is very valuable for designing heat sinks. Similarly, it can be seen from Fig. 5(b, c) that in the range of the mass of 1—1.5 kg and junction temperature of 60—70 ℃, they continue to decrease, but the increase of the cost is not obvious. These are worthy of our attention. In addition, only pursuing the reduction of temperature and mass will lead to a substantial increase in cost, which should be avoided during the design process.

In the Pareto frontier solution, the junction temperature of S_{a4} is far less than the maximum allowable temperature of 125 ℃, which meets the restriction requirements. Comparing Fig.6(a) and Fig.6(b), we find the Pareto solution set after the normalization of the objective function has a more uniform distribution and can provide a better compromise solution.

4.3 Comparison with the NSGA-Ⅱ algorithm

To verify the effectiveness of the algorithm in this paper, the widely used NSGA-Ⅱ algorithm[13] is used to solve the same problem. To control the variables, we set the population size and number of iterations of NSGA-Ⅱ to be consistent with those of MOEA/D. The crossover probability and mutation probability are 0.9 and 0.2, respectively, and the optimal frontier of Pareto is shown in Fig.7.

Comparing Fig. 6(b) and Fig. 7, we can find that the optimal frontier distribution of the NSGA-Ⅱ algorithm is very discontinuous, indicating that the satisfaction of each solution is different. This is because the algorithm's optimization search is random, whether the points on the actual optimal frontier surface are continuous depends on the size of the population. When the population size tends to be infinite, it will be completely consistent with the actual optimal frontier surface, but it will consume a lot of memory and time.

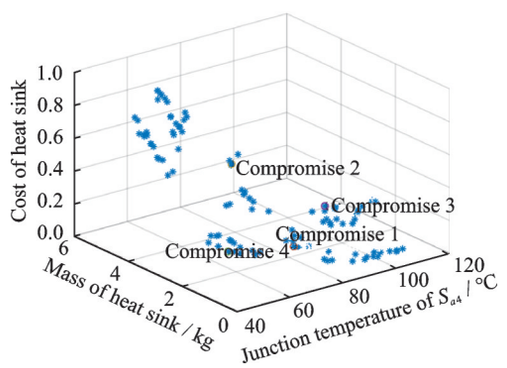

Fig.7 Pareto optimal frontier of NSGA-Ⅱ algorithm

With the same calculation circumstances, the solution time of NSGA-Ⅱ is 7.248 8 s, which is twice of the MOEA/D (3.610 3 s). In Fig.8, the optimization results of the two algorithms for compromise solution 1 are counted 20 consecutive

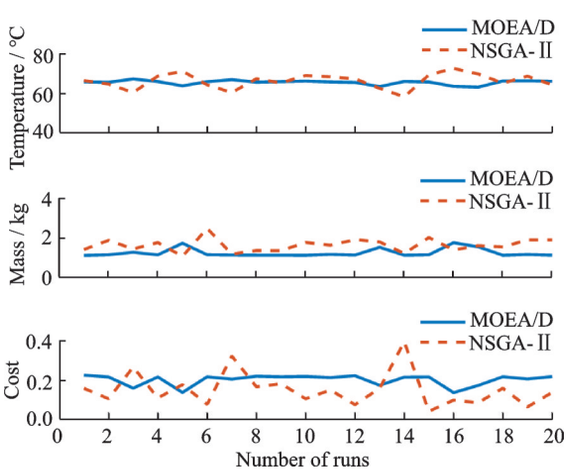

Fig.8 Comparison of the robustness of two algorithms

times. It can be clearly seen that the compromise solution provided by MOEA/D is relatively stable and reliable. Therefore, from the perspective of the continuity of the Pareto frontier, the rapidity and robustness of the algorithm, the results of MOEA/D reflect its superiority in the thermal optimization problem.

5 Simulation

We use the software ANSYS Icepak to model the results of the four compromise solutions of MOEA/D, set the power device S_{a4} as the temperature monitoring point, and get its average temperature.

As shown in Table 3, the error is smaller compared with the theoretical calculation value, indicating that the proposed method is accurate and effective. Among them, solution 2 is that the fins are arranged densely and the heat dissipation area increases, which reduces the junction temperature. However, due to the thermal shielding between the fins, the radiation capacity is reduced, which leads to heat building up during simulation. So the simulation results are quite different from the model calculated results.

Table 3 Comparison of simulation results and model optimization results

Result	Optimized value/℃	Simulation value/℃	Error/%
Compromise 1	66.061 6	66.7	0.97
Compromise 2	54.711 9	56.9	3.99
Compromise 3	64.816 0	65.2	0.59
Compromise 4	69.324 3	70.5	0.17

It can be seen from Fig.9 that the temperature cloud image of S_{a4} does not fall in a circular gradient from the center to the periphery, indicating that there is a thermal coupling phenomenon between the chips. Therefore, all the simulation results are slightly higher than the calculated temperatures. In solution 4, the thermal coupling phenomenon is weakened because of the larger area of the substrate and the increased distance between the chips, so the error of the result is the lowest.

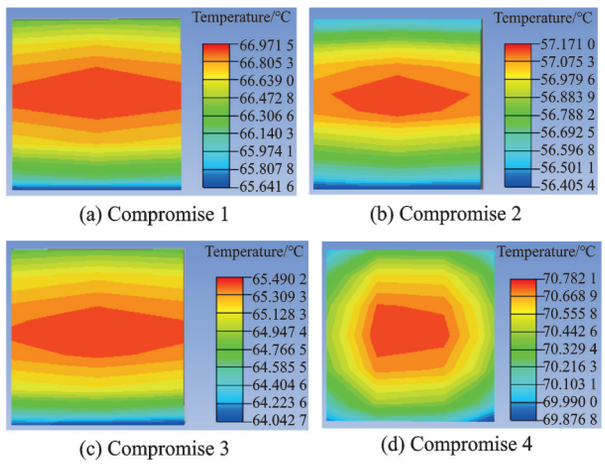

Fig.9 S_{a4} temperature distribution cloud map

6 Conclusions

Aiming at the multi-objective thermal design problem of dual-input ASI, the improved MOEA/D proposed in this paper has good advantages.

(1) After the objective function is normalized, the solution distribution on the MOEA/D optimal frontier is more uniform. Combined with the evaluation method of fuzzy set theory, the mass of each objective can be dynamically adjusted to meet users' different needs and obtain different compromise solutions.

(2) Taking junction temperature of the power device, mass and cost of the heat sink as the optimization goals, the algorithm is applied to the thermal design of the dual-input ASI. The optimization result meets the temperature rise requirement of the power device, and the mass and cost of the heat sink are improved.

(3) Compared with the classic multi-objective optimization algorithm NSGA-Ⅱ, the Pareto frontier solution of the algorithm in this paper has better continuity; the solution time is reduced by half; and the solution results are more stable for 20 consecutive times. It has better rapidity and robustness.

The method combining MOEA/D and the fuzzy set theory proposed in this paper can be used for the thermal design of aviation equipment, and extended to other engineering designs.

References

[1] ZHANG Fanghua, GONG Chunying, DENG Xiang. Review of aeronautic static inverter[J]. Journal of Nanjing University of Aeronautics & Astronautics, 2014, 46(1): 19-26.(in Chinese)

[2] LI Shang, GE Hongjuan, YIN Hang, et al. Three-phase aeronautical static inverter based on dual-input bi-direction pulsating voltage source cells[J]. Transactions of China Electrotechnical Society, 2021, 36(16): 3493-3503. (in Chinese)

[3] ZHAO D. Thermal design of electronic equipment [M]. Beijing: Electronics Industry Press, 2009.

[4] ZHOU Zhenkai, LIU Bing, WAN Yangtao, et al. Optimization design of heat sink fins based on genetic algorithm[J]. Electro-Mechanical Engineering, 2019, 35(5): 29-33. (in Chinese)

[5] LIU Bei, CHEN Jie, SU Da. Structure optimization design of phase change radiator[J]. Journal of Machine Design, 2020, 37(S1): 270-273. (in Chinese)

[6] LI Jian, LU Fanli, DONG Wei, et al. Structure optimization of chip cooling radiator based on numerical simulation[J]. Journal of Shanghai Jiaotong University, 2019, 53(4): 461-467. (in Chinese)

[7] ZHAO N, WANG L. Optimal design of helicopter oil radiator based on genetic algorithm[J]. Journal of Machine Design, 2014, 31(1): 36-41.

[8] HU Jianhui, LI Jingeng, ZOU Jibin, et al. Losses calculation of IGBT module and heat dissipation system design of inverters[J]. Transactions of China Electrotechnical Society, 2009, 24(3): 159-163. (in Chinese)

[9] LEE S, SONG S, AU V, et al. Constriction/spreading resistance model for electronics packaging[C]// Proceedings of ASME/JSME Thermal Engineering Conference.[S.l.]:[s.n.], 1995:199-206.

[10] ZHANG Q, LI H, MARINGER D, et al. MOEA/D with NBI-style Tchebycheff approach for portfolio management[C]//Proceedings of IEEE Congress on Evolutionary Computation. Barcelona, Spain: IEEE, 2010:1-8.

[11] ZHU Yongsheng, WANG Jie, QU Boyang, et al. Environmental economic dispatch adopting multi-objective evolutionary algorithm based on decomposition[J]. Power System Technology, 2014, 38(6): 1577-1584. (in Chinese)

[12] PAL S, QU B, DAS S, et al. Linear antenna array synthesis with constrained multi-objective differential evolution[J]. Progress in Electromagnetics Research, B 2010, 21: 87-111.

[13] DEB K, PRATAP A, AGARWAL S, et al. A fast and elitist multi-objective genetic algorithm: NSGA-Ⅱ[J]. IEEE Transactions on Evolutionary Computation, 2002, 6(2): 182-197.

Acknowledgements This work was supported by the National Natural Science Foundation of China (Nos. U1933115, U2133203).

Authors Ms. **YAN Jie** received her B.S. degree in aircraft airworthiness technology from Nanjing University of Aeronautics and Astronautics (NUAA), China, in 2020, where she is currently pursuing the M.S. degree in airworthiness technology and management. Her current research interest includes electronic device thermal design and airborne systems network safety.

Prof. **GE Hongjuan** received her B.S. and M.S. degrees in electrical engineering from Southeast University, Nanjing, China, in 1985 and 1988, respectively, and the Ph.D. degree in electric machines and electric apparatus from NUAA, China, in 2006. She is currently a full professor with College of Civil Aviation, NUAA. Her current research interests include the space-vector control of PWM, AC-AC converters, and airworthiness technology.

Author contributions Ms. **YAN Jie** designed the study, complied the models, conducted the analysis, interpreted the results and wrote the manuscript. Prof. **GE Hongjuan** checked the content of the manuscript for correctness and plausibility, and suggested revisions. Dr. **WANG Yongshuai** contributed to theoretical basis for the analysis. Dr. **LI Huang** contributed to build the simulation model of the cooling system. All authors commented on the manuscript draft and approved the submission.

Competing interests The authors declare no competing interests.

(Production Editor: ZHANG Bei)

基于MOEA/D的双输入航空静止变流器多目标热优化

闫 洁[1], 葛红娟[1], 王永帅[2], 李 煌[1]

(1.南京航空航天大学民航学院,南京 211106,中国; 2.南京航空航天大学自动化学院,南京 211106,中国)

摘要:提出基于MOEA/D和模糊集理论相结合的优化方法,解决双输入航空静止变流器热设计过程中多变量多目标的寻优问题。分析功率器件的传热路径并构建等效热路,以功率器件结温、散热器质量、散热器成本为优化目标,以散热器的结构参数为设计变量,基于MOEA/D开展热优化。本文进行了比较研究,结果表明所提出的算法不仅能够满足多目标权重的不同要求,且快速性和鲁棒性好。

关键词:航空静止变流器;热优化;散热器;MOEA/D;模糊集理论